International Journal of Pavement Engineering
Vol. 13, No. 4, August 2012, 322–338

Taylor & Francis
Taylor & Francis Group

Comparing finite element and constitutive modelling techniques for predicting rutting of asphalt pavements

Rashid K. Abu Al-Rub[a]*, Masoud K. Darabi[a], Chien-Wei Huang[b], Eyad A. Masad[a,b] and Dallas N. Little[a]

[a]*Zachry Department of Civil Engineering, Texas A&M University, College Station, TX 77843, USA;* [b]*Mechanical Engineering Program, Texas A&M University at Qatar, Doha, Qatar*

(*Received 17 May 2010; final version received 23 February 2011*)

This paper focuses on a comprehensive evaluation of the effects of different finite element (FE) modelling techniques and material constitutive models on predicting rutting in asphalt pavements under repeated loading conditions. Different simplified 2D and more realistic 3D loading techniques are simulated and compared for predicting asphalt rutting. This study also evaluates and compares the rutting performance predictions using different material constitutive behaviours such as viscoelastic–viscoplastic, elasto-viscoplastic and coupled viscoelastic, viscoplastic and viscodamage behaviours. The simulations show that the assumption of the equivalency between a pulse loading and an equivalent loading, which are commonly used as simplified loading assumptions for predicting rutting, is reasonable for viscoelastic–viscoplastic and elasto-viscoplastic constitutive behaviours. However, these loading assumptions and material constitutive models overestimate rutting as damage grows. Results show that the 2D plane strain FE simulations significantly overestimate rutting as compared with the rutting performance predictions from more realistic 3D FE simulations.

Keywords: rutting; viscoelasticity; viscoplasticity; damage; finite element simulations; wheel loading

1. Introduction

Rutting is one of the most serious distresses in asphalt pavements affecting the pavement performance and service life. Therefore, the accurate simulation of rutting in asphalt pavements is essential for improving their performance and management. The main mechanism of rutting is the accumulation of permanent deformation that increases progressively with increasing number of loading cycles. However, the complex nature of the applied loading conditions, very large number of loading cycles (millions of loading cycles) and complex constitutive behaviour of asphaltic materials make the accurate prediction of rutting a very difficult and challenging task. Even with the current state-of-the-art in computational power, conducting 3D finite element (FE) rutting performance simulations for pavements subjected to millions of wheel loading cycles and considering realistic wheel tracking and environmental loading conditions is almost impossible. Therefore, an evaluation of a simplified numerical model with efficient and realistic loading conditions and material constitutive models that can simulate the pavement rutting performance for a very large number of loading cycles is desirable. In order to accurately simulate the pavement response, the computer simulations should have the capability to capture the response by considering structural loading, boundary conditions and material constitutive behaviour. Therefore, realistic loading and boundary conditions should be imposed, and an accurate material constitutive model should be utilised. The material model should be able to describe the inelastic damage behaviour of asphalt under different stress levels, loading rates and temperatures.

At the material level, the experimental measurements show that the deformation response of asphaltic materials can be decomposed into recoverable (viscoelastic) and irrecoverable (viscoplastic) deformations that are temperature, stress and strain-rate dependent (e.g. Perl *et al.* 1983, Sides *et al.* 1985, Collop *et al.* 2003). For predicting the recoverable deformation, Huang *et al.* (2007) and Masad *et al.* (2008) have employed Schapery's single integral nonlinear viscoelastic model (Schapery 1969) to characterise the nonlinear viscoelastic behaviour of asphalt mixtures and binders. They have implemented Schapery's viscoelastic model into the well-known commercial FE code Abaqus (2008) through the user material subroutine UMAT utilising the recursive iterative numerical algorithm by Haj-Ali and Muliana (2004). Several other researches (e.g. Sadd *et al.* 2004, Abu Al-Rub *et al.* 2009, Masad *et al.* 2009, Saadeh and Masad 2010) also used Schapery's nonlinear viscoelastic model for analytically predicting the viscoelastic response of asphalt materials. Masad *et al.* (2009) and Abu Al-Rub *et al.* (2009) have developed a systematic procedure to characterise and decouple the recoverable (viscoelastic) and irrecoverable (viscoplastic) deformations by analysing repeated creep-recoverable experimental tests using

*Corresponding author. Email: rabualrub@civil.tamu.edu

ISSN 1029-8436 print/ISSN 1477-268X online

http://dx.doi.org/10.1080/10298436.2011.566613
http://www.tandfonline.com

Schapery's nonlinear viscoelastic model. On the other hand, the irrecoverable (viscoplastic) deformations in asphaltic materials are commonly predicted using the Perzyna's (1971) viscoplastic model (e.g. Lu and Wright 1998, Seibi *et al.* 2001, Masad *et al.* 2005, 2007, Huang 2008, Abu Al-Rub *et al.* 2009). Huang (2008), Huang *et al.* (2011) and Abu Al-Rub *et al.* (2009) have coupled Schapery's nonlinear viscoelastic model and Perzyna's viscoplastic model and validated the coupled model against a large number of creep-recovery experimental data obtained at different stress levels, loading times and temperatures. However, the changes in the material's microstructure during deformation cause asphaltic materials to experience a significant amount of micro-damage (in the form of micro-cracks and micro-voids) under service loading conditions such that tertiary creep, post-peak behaviour of the stress–strain response and degradation in the mechanical properties could not be explained only by viscoelasticity and viscoplasticity constitutive models. Also, it is believed that damage significantly contributes to the amount of rutting observed in experimental studies. Hence, the inclusion of damage in the constitutive equations of asphaltic materials seems inevitable. It should be noted that Schapery's viscoelastic damage model (Schapery 1975, 1987), which has been modified by Schapery (1999) to include viscoplasticity, is currently used to reasonably predict the damage behaviour of asphaltic materials (e.g. Lee and Kim 1998; Chehab 2002; Chehab *et al.* 2002, 2003; Kim and Chehab 2002; Gibson *et al.* 2003; Gibson 2006; Underwood *et al.* 2006; Kim *et al.* 2007; Sullivan 2008 and the reference quoted therein). Recently, Darabi *et al.* (2011a) proposed a damage law for asphaltic materials and coupled it to Schapery's nonlinear viscoelasticity and Perzyna's visco-plasticity models to describe the response of asphaltic materials under different loading conditions and temperatures. The model was successfully validated through comparing the model predictions with experimental data obtained at different loading conditions (e.g. creep-recovery, creep and constant strain-rate loadings), stress levels, strain rates and temperatures. Later Abu Al-Rub *et al.* (2010a) enhanced this model by incorporating a micro-damage healing model to capture the fatigue behaviour of asphalt mixtures more accurately. The model presented by Darabi *et al.* (2011a) is summarised in this paper and is utilised for conducting the rutting performance simulations.

In terms of the FE modelling of asphaltic pavements under simplified loading conditions, several FE studies have been conducted in order to predict the rutting performance. Lu and Wright (1998) constructed a 2D plane strain FE model to represent a three-layer pavement structure and employed the Perzyna's viscoplastic model to predict the permanent deformation under large number of loading cycles assuming a pulse loading. Pulse loading is commonly used to represent a wheel moving load. However, the implicit assumption in conducting 2D plane strain FE simulations is that the loading condition is represented as an infinite load strip in the traffic direction (see Table 1). Similarly, Hunter *et al.* (2007) have also conducted 2D plane strain FE simulations of the wheel tracking test in order to predict rutting performance assuming a pulse loading. However, Hunter *et al.* (2007) have used a power law viscoplasticity constitutive model and neglected viscoelasticity and damage evolution. Their simulations show that the shape of rutting is significantly different from that obtained experimentally. Kettil *et al.* (2007) have conducted 2D axisymmetric FE simulations and compared two different loading assumptions: pulse loading and equivalent loading (see Table 1). The equivalent loading assumption, which is another commonly adapted loading assumption to represent a wheel moving load, applies the wheel loading over the respective accumulative loading time neglecting the unloading time periods. Results from this study showed that the equivalent loading assumption gives comparable rutting performance predictions from the pulse loading assumption such that by assuming an equivalent loading, one can save significant amount of computational time. However, this conclusion is based on assuming elasto-viscoplastic material behaviour and neglecting the viscoelastic and damage behaviour of asphaltic materials. Cho *et al.* (1996) compared the rutting predictions from 2D plane strain, 2D axisymmetric and 3D FE simulations assuming a linear elastic behaviour of the asphalt material. Huang *et al.* (2001) conducted 2D and 3D axisymmetric simulations of asphalt pavement sections using an elasto-viscoplastic model. Results of this research showed that the 3D FE analysis gives more accurate predictions as than field measurements. Huang (1995) proposed a step loading function to simulate a large number of loading cycles of a moving load in 3D FE simulations. This loading function accumulates each wheel pass time to produce a total cumulative loading time and then applies a single load step to a set of elements in the middle of the whole wheel path. Hua (2000) improved the cumulative loading time approach by Huang (1995). The improved approach also accumulates each single loading time, and then applies a single step loading on the whole wheel path to represent the moving wheel loading in 3D simulations. However, in both of these works (i.e. Huang 1995, Hua 2000), an elasto-viscoplastic model is used for validating the proposed loading models. Park *et al.* (2005), Hua and White (2002) and Huang *et al.* (2001) used an elasto-viscoplastic model along with the cumulative loading time approach to represent a large number of loading cycles. Saleeb *et al.* (2005) used a visco-elastoplastic model to conduct a 3D FE simulation with a moving loading model by applying the loading on one set of elements and then moving forward to the next set of elements. However, most of the aforementioned FE

Table 1. Summary of simulated loading assumptions.

Mode	Loading approach	Loading area	Schematic representation of loading modes
1 (2D)	Pulse loading (plane strain)	One wheel	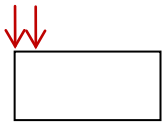
2 (2D)	Equivalent loading (plane strain)	One wheel	
3 (2D)	Pulse loading (axisymmetric)	One wheel	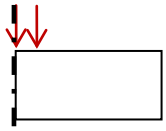
4 (2D)	Equivalent loading (axisymmetric)	One wheel	
5 (3D)	Pulse loading	One wheel	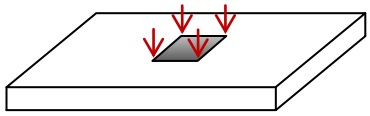
6 (3D)	Equivalent loading	One wheel	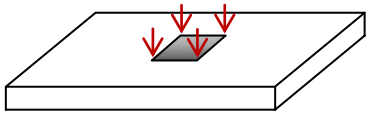
7 (3D)	Pulse loading	Whole wheel path	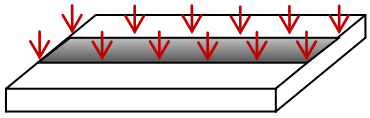
8 (3D)	Equivalent loading	Whole wheel path	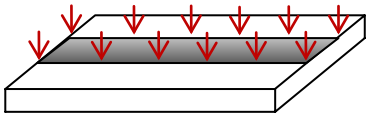
9 (3D)	Pulse loading	Circular loading area	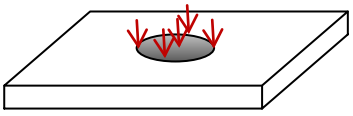
10 (3D)	Equivalent loading	Circular loading area	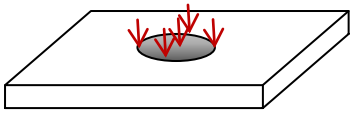
11 (3D)	Moving loading	One wheel	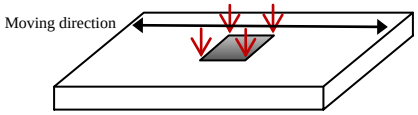

simulations have focused on the effect of loading modes. To the authors' best knowledge, no study has yet used a comprehensive constitutive model incorporating nonlinear viscoelasticity, viscoplasticity and viscodamage for simulating rutting performance of asphalt pavements.

The main objective of this paper is to study the effect of different simplified wheel loading assumptions on 2D and 3D FE rutting simulations of asphalt layers using different constitutive behaviours; namely elasto-visco-plastic, viscoelastic–viscoplastic and coupled viscoelastic–viscoplastic–viscodamage constitutive behaviours.

Different simplified 2D and more realistic 3D FE loading techniques that represent the commonly conducted wheel tracking test are simulated and compared with predict asphalt rutting performance.

2. Material constitutive model

In this section, the coupled nonlinear viscoelastic–viscoplastic–viscodamage constitutive model that has been recently presented and validated by Darabi *et al.* (2011a) is recapped. Different simplified assumptions of this constitutive model are used to represent various types of constitutive models. For example, one can simplify the general constitutive model to represent an elasto-viscoplastic model neglecting the transient response in viscoelasticity and neglecting damage evolution. In fact, it is possible to turn on/off any of the components of the constitutive model such as linear/nonlinear viscoelasticity, viscoplasticity and viscodamage. This allows one to investigate the effect of different constitutive assumptions on rutting prediction of asphaltic layers.

In general, the total strain of asphalt mixtures under loading can be decomposed into recoverable (viscoelastic) and irrecoverable (viscoplastic) components, such that

$$\varepsilon_{ij} = \varepsilon_{ij}^{\mathrm{ve}} + \varepsilon_{ij}^{\mathrm{vp}}, \tag{1}$$

where $\boldsymbol{\varepsilon}$ is the total strain tensor, $\boldsymbol{\varepsilon}^{\mathrm{ve}}$ is the viscoelastic strain tensor and $\boldsymbol{\varepsilon}^{\mathrm{vp}}$ is the viscoplastic strain tensor.

Once the material is damaged, the load is carried out by the undamaged (effective or intact) material. Hence, viscoelasticity and viscoplasticity constitutive equations should be expressed in terms of the effective (true) stresses $\bar{\sigma}_{ij}$ instead of the nominal (apparent) stresses σ_{ij} (Abu Al-Rub and Voyiadjis 2003). Therefore, one can express the effective stresses $\bar{\sigma}_{ij}$ in terms of the nominal (damaged) stresses σ_{ij} using the following equation [one can refer to Chaboche (2003) for more details on damage mechanics theories]:

$$\bar{\sigma}_{ij} = \frac{\sigma_{ij}}{1-\phi}, \tag{2}$$

where $0 \le \phi \le 1$ is the damage density (representing the area of micro-cracks and micro-voids per unit area) such that $\phi = 0$ when there is no damage and $\phi = 1$ when the material is completely damaged. The superscript ' $-$ ' in the above equation and in the subsequence represents the effective (undamaged) configuration. As mentioned before, the common argument in the continuum damage mechanics theories is that once the material is damaged, further loading can only affect the undamaged material skeleton. Hence, the viscoelastic, viscoplastic and viscodamage models are defined as a function of variables in the effective configuration.

However, a transformation hypothesis is required to relate the nominal stress and strain tensors ($\boldsymbol{\sigma}$ and $\boldsymbol{\varepsilon}$) to the stress and strain tensors in the effective configuration ($\bar{\boldsymbol{\sigma}}$ and $\bar{\boldsymbol{\varepsilon}}$). For simplicity and easiness in the FE implementation, the strain equivalence hypothesis is adopted. Hence, one can assume that the nominal strain tensors $\boldsymbol{\varepsilon}$, $\boldsymbol{\varepsilon}^{\mathrm{ve}}$ and $\boldsymbol{\varepsilon}^{\mathrm{vp}}$ are equal to their counterparts in the effective configuration, $\bar{\boldsymbol{\varepsilon}}$, $\bar{\boldsymbol{\varepsilon}}^{\mathrm{ve}}$ and $\bar{\boldsymbol{\varepsilon}}^{\mathrm{vp}}$, such that

$$\varepsilon_{ij} = \bar{\varepsilon}_{ij}, \quad \varepsilon_{ij}^{\mathrm{ve}} = \bar{\varepsilon}_{ij}^{\mathrm{ve}}, \quad \varepsilon_{ij}^{\mathrm{vp}} = \bar{\varepsilon}_{ij}^{\mathrm{vp}}. \tag{3}$$

The viscoelastic strain tensor, $\bar{\boldsymbol{\varepsilon}}^{\mathrm{ve}}$, can be described using Schapery's nonlinear viscoelasticity theory (Schapery 1969). Assuming small deformations, Schapery's viscoelastic 1D integral model, which is written in this study in terms of the effective stress, $\bar{\sigma}$, is given by

$$\bar{\varepsilon}^{ve,t} = g_0 \bar{D}_0 \bar{\sigma}^t + g_1 \int_0^{\psi} \Delta\bar{D}\left(\psi^t - \psi^\tau\right) \frac{\mathrm{d}\left(g_2 \bar{\sigma}^\tau\right)}{\mathrm{d}\tau} \mathrm{d}\tau, \tag{4}$$

where the superscript 't' represents the time at which the strain is predicted; $\bar{D}_0$ is the instantaneous compliance, which represents the elastic response; $\Delta\bar{D}$ is the transient compliance, which describes the time-dependent response; g_0, g_1 and g_2 are nonlinear parameters that can be a function of stress (when $g_0 = g_1 = g_2$ a linear viscoelastic strain is obtained) and ψ^t is the reduced time which can be a function of temperature, stress and other environmental factors (e.g. moisture and ageing) and is given by

$$\psi^t = \int_0^t \frac{\mathrm{d}\xi}{a_{\mathrm{T}} a_{\mathrm{s}} a_{\mathrm{e}}}, \tag{5}$$

where a_{T} is the time–temperature shift factor, a_{s} is the stress shift factor and a_{e} is the environmental shift factor. It should be noted that several researchers have included a_{e} in the definition of ψ^t in order to investigate the viscoelastic response of materials in the presence of environmental effects such as the moisture that leads to moisture-induced damage and oxygen that leads to ageing. To name a few, Muliana and Haj-Ali (2004) and Masad *et al.* (2008) employed the ageing shift factor to model the behaviour of aged and unaged polymeric composites and asphalt mixtures, respectively. Chen *et al.* (1993) and Pappas and Rao (1989) used the moisture shift factor to study the effect of moisture on viscoelastic response of composite laminates and biomaterials, respectively. However, further investigations are still required to investigate the accurate coupling between the viscoelastic response of materials and the environmental conditions such as ageing and moisture. Recently, Abu Al-Rub *et al.* (2010b) have presented a new approach for incorporating the effect of moisture-induced damage on the viscoelastic response of asphalt mixtures. This approach will be adapted in a future work in order to investigate the effect of

moisture-induced damage on the rutting performance of asphalt pavements.

The Prony series is employed to represent the transient compliance $\Delta\bar{D}$ as follows:

$$\Delta\bar{D}^{\psi^t} = \sum_{n=1}^{M} \bar{D}_n\left[1 - \exp\left(-\lambda_n\psi^t\right)\right], \tag{6}$$

where $\bar{D}_n$ is the nth coefficient of Prony series associated with the nth retardation time λ_n, and M is the number of Prony series components. Once all the components of $\bar{D}_n$ equal to 0, the model represents the elastic time-independent strain.

For 3D isotropic constitutive relations, the viscoelastic strain can be decoupled into deviatoric and volumetric components as follows:

$$\bar{\varepsilon}_{ij}^{\text{ve}} = \bar{e}_{ij}^{\text{ve}} + \frac{1}{3}\bar{\varepsilon}_{kk}\delta_{ij} = \frac{\bar{J}}{2}\bar{S}_{ij} + \frac{\bar{B}}{3}\bar{\sigma}_{kk}\delta_{ij}, \tag{7}$$

where $\bar{\boldsymbol{e}}^{\text{ve}}$ is the deviatoric component of the viscoelastic strain tensor and $\bar{\varepsilon}_{kk}^{\text{ve}}$ is the volumetric viscoelastic strain; $\bar{J}$ and $\bar{B}$ are the undamaged shear and bulk compliances, respectively; $\bar{S}_{ij} = \bar{\sigma}_{ij} - \bar{\sigma}_{kk}\delta_{ij}/3$ are the components of the deviatoric effective stress tensor; δ_{ij} is the Kronecker delta and $\bar{\sigma}_{kk}$ is the volumetric part of the effective stress. Applying Schapery's integral constitutive model of Equation (4), the deviatoric and volumetric viscoelastic strain components can be expressed, respectively, as follows:

$$\bar{e}_{ij}^{ve,t} = \frac{1}{2}g_0^t\bar{J}_0\bar{S}_{ij}^t + \frac{1}{2}g_1^t\int_0^t \Delta\bar{J}^{(\psi^t-\psi^\tau)}\frac{\mathrm{d}(g_2^\tau\bar{S}_{ij}^\tau)}{\mathrm{d}\tau}\mathrm{d}\tau \quad \text{and} \tag{8}$$

$$\bar{\varepsilon}_{kk}^{ve,t} = \frac{1}{3}g_0^t\bar{B}_0\bar{\sigma}_{kk}^t + \frac{1}{3}g_1^t\int_0^t \Delta\bar{B}^{(\psi^t-\psi^\tau)}\frac{\mathrm{d}(g_2^\tau\bar{\sigma}_{kk}^\tau)}{\mathrm{d}\tau}\mathrm{d}\tau, \tag{9}$$

where $\bar{J}_0$ and $\bar{B}_0$ are the instantaneous undamaged elastic shear and bulk compliances, respectively.

It is noteworthy that Darabi *et al.* (2011b) derived the temperature-dependent Schapery-type nonlinear viscoelastic model based on the principles of thermodynamics. They have shown that the time–temperature shift factor a_{T} can be incorporated in the viscoelasticity model either through the reduced time ψ^t or through the retardation time coefficients λ_n. They also showed that incorporating the time–temperature shift factor through the retardation time coefficients significantly simplifies the expression for the thermo-mechanical coupling terms. Here, a similar approach is used such that one can write

$$\lambda_n = \lambda_n^0 \exp\left[-\delta\left(1 - \frac{T}{T_0}\right)\right], \tag{10}$$

where λ_n^0 is the retardation time at reference temperature T_0 and δ is the viscoelasticity temperature-coupling material parameter. Therefore, substituting Equation (10) into Equation (6) along with Equation (5), one may conclude that time is divided by the time–temperature shift factor $a_{\text{T}} = \exp\left[\delta(1 - T/T_0)\right]$ to give the standard reduced time. However, in this work, an Arrhenius-type function, Equation (10), is assumed to model the effect of temperature on the viscoelastic response of asphalt mixtures. Equation (10) assumes that the natural logarithm of the temperature-coupling term (or of the time–temperature shift factor) has a linear relationship with temperature (i.e. $\ln a_{\text{T}} = \delta(1 - T/T_0)$). This assumption may not be valid for a wide range of temperatures. However, this approximation is adapted here due to the lack of experimental data at different temperatures.

The viscoplastic strain tensor, $\bar{\boldsymbol{\varepsilon}}^{\text{vp}}$, can be described by a Perzyna-type viscoplasticity theory (Perzyna 1971) such that the rate of the viscoplastic strain is expressed as follows:

$$\dot{\bar{\varepsilon}}_{ij}^{\text{vp},t} = \dot{\bar{\gamma}}^{\text{vp}}\frac{\partial g}{\partial\bar{\sigma}_{ij}}, \tag{11}$$

where the superimposed dot designated the derivative with respect to time, $\dot{\bar{\gamma}}^{\text{vp}}$, is the viscoplastic multiplier and g is the viscoplastic potential function. Experimental measurements demonstrated that asphalt mixtures exhibit non-associative viscoplastic response such that the use of an associative flow rule overestimates the volumetric strain of an asphaltic material (Masad *et al.* 2005, 2007). Hence, the non-associated viscoplasticity is used here. Thus, the viscoplastic potential g is different from the yield surface f. In this study, the following expressions are postulated for the viscoplastic potential and yield surface:

$$g = \bar{\tau} - \beta\bar{I}_1, \tag{12}$$

$$f = \bar{\tau} - \alpha\bar{I}_1 - \kappa\left(\bar{\varepsilon}_e^{\text{vp}}, T\right), \tag{13}$$

where α and β are material parameters related to the material's internal friction; $\kappa\left(\bar{\varepsilon}_e^{\text{vp}}, T\right)$ is the temperature-dependent isotropic hardening function which depends on the effective viscoplastic strain $\bar{\varepsilon}_e^{\text{vp}}$ and temperature T; $\bar{I}_1 = \bar{\sigma}_{kk}$ is the first invariant of the effective stress tensor $\bar{\boldsymbol{\sigma}}$ and $\bar{\tau}$ is an equivalent measure of the deviatoric shear stress in the effective configuration, which is expressed as follows:

$$\bar{\tau} = \frac{\sqrt{3\bar{J}_2}}{2}\left[1 + \frac{1}{d} + \left(1 - \frac{1}{d}\right)\frac{3\bar{J}_3}{\sqrt{3\bar{J}_2^3}}\right], \tag{14}$$

where $\bar{J}_2 = 1/2\bar{S}_{ij}\bar{S}_{ij}$ and $\bar{J}_3 = 1/2\bar{S}_{ij}\bar{S}_{jk}\bar{S}_{ki}$ are the second and third deviatoric invariants of the effective stress, $\bar{\boldsymbol{\sigma}}$, respectively, and d is a material parameter that considers the distinction of asphalt mixture behaviour in compression and extension loading conditions.

Using Perzyna's (1971) theory of viscoplasticity, one can postulate the following form for the viscoplastic multiplier $\dot{\bar{\gamma}}^{\mathrm{vp}}$:

$$\dot{\bar{\gamma}}^{\mathrm{vp}} = \Gamma^{\mathrm{vp}}(T)\langle \Phi(f)\rangle^{N}, \tag{15}$$

where Γ^{vp} is the temperature-dependent viscoplasticity viscosity parameter, Φ is the overstress function which is expressed in terms of the yield function f, N is the strain-rate exponent and the symbol $\langle\,\rangle$ is the MacAulay bracket defined by $\langle x\rangle = (x + |x|)/2$. In this work, the following forms are postulated for the overstress function and the temperature-dependent viscoplasticity viscosity parameter (Darabi *et al.* 2011b):

$$\Phi(f) = \frac{f}{\bar{\tau} - \alpha \bar{I}_1}, \tag{16}$$

$$\Gamma^{\mathrm{vp}}(T) = \Gamma_0^{\mathrm{vp}} \exp\left[-\delta\left(1 - \frac{T}{T_0}\right)\right], \tag{17}$$

where Γ_0^{vp} is the viscoplastic viscosity at the reference temperature T_0.

Moreover, an exponential function for the isotropic hardening function $\kappa\left(\bar{\varepsilon}_e^{\mathrm{vp}}, T\right)$ in Equation (13) can be assumed following the work of Lemaitre and Chaboche (1990), such that

$$\kappa = \left[\kappa_0 + \kappa_1\left(1 - \exp\left(-\kappa_2 \bar{\varepsilon}_e^{\mathrm{vp}}\right)\right)\right] \exp\left[-\delta\left(1 - \frac{T}{T_0}\right)\right], \tag{18}$$

where κ_0, κ_1 and κ_2 are material parameters defining the initial yield stress, the saturated yield stress and the strain hardening rate, respectively, at the reference temperature T_0. Also, one can easily show that the rate of the effective viscoplastic strain $\dot{\bar{\varepsilon}}_e^{\mathrm{vp}}$ can be expressed as follows (Huang 2008):

$$\dot{\bar{\varepsilon}}_e^{\mathrm{vp}} = A^{-1}\sqrt{\dot{\bar{\varepsilon}}_{ij}^{\mathrm{vp}}\dot{\bar{\varepsilon}}_{ij}^{\mathrm{vp}}} \quad \text{where } A = \sqrt{1 + 2\left(\frac{0.5 + \beta/3}{1 - \beta/3}\right)^2}. \tag{19}$$

In order to calculate the effective stress in Equation (2), the damage density ϕ should be calculated. In this work, we employ the thermo-viscodamage model proposed by Darabi *et al.* (2011a) to model the damage response of asphaltic materials. They formulated the viscodamage model to be a function of temperature, total effective strain and damage driving force, which is expressed in terms of the stress invariants of the effective stress in the undamaged configuration. The expression for the proposed damage force is assumed analogous to $\bar{\tau}$ in Equation (14) in order to consider the confinement effects on the damage response of asphaltic materials and to allow for the distinction between the influence of compression and extension loading conditions on damage nucleation and growth. The viscodamage model in presented as follows:

$$\dot{\phi} = \Gamma_0^{\mathrm{vd}}\left[\frac{\bar{Y}}{Y_0}\right]^{q}(1 - \phi)^2 \exp\left(k\bar{\varepsilon}_{\mathrm{e}}\right) \exp\left[-\xi\left(1 - \frac{T}{T_0}\right)\right], \tag{20}$$

where Y_0, Γ_0^{vd}, q, k and ξ are damage material parameters that are obtained at the reference temperature, T_0; $\bar{\varepsilon}_{\mathrm{e}}$ is the effective total strain $\bar{\varepsilon}_{\mathrm{e}} = \sqrt{\bar{\varepsilon}_{ij}\bar{\varepsilon}_{ij}}$; T is the temperature and $\bar{Y}$ is the damage driving force which is assumed to have the same expression as $\bar{\tau}$ in Equation (14) (i.e. $\bar{Y} = \bar{\tau}$).

It is noteworthy that the viscodamage model is implemented using the effective configuration concept, which avoids the complexities associated with the direct couplings of the viscoelastic and viscoplastic models to the damage model. In other words, one can calculate the effective stress and strain tensors using the viscoelastic and viscoplastic models, and then, use the effective variables to calculate the damage evolution presented in Equation (20). Finally, the nominal stress tensor can be updated using Equation (2). It should also be noted that the effective stress tensor increases as the damage density increases. Consequently, the inclusion of the damage model affects both the viscoelastic and viscoplastic behaviours.

The presented nonlinear viscoelastic–viscoplastic–viscodamage model has been implemented into the well-known commercial FE software Abaqus (2008) via the user material subroutine UMAT. The reader is referred to Abu Al-Rub *et al.* (2009) for the details of the numerical implementation. Also, the model has been validated by Huang *et al.* (2007), Darabi *et al.* (2011a) and Abu Al-Rub *et al.* (2009, 2010a) against a large set of experimental data for creep-recovery, creep and constant strain-rate tests over a range of temperatures, stress levels and strain rates.

3. Description of the FE simulations

This section presents the description of 2D and 3D FE rutting simulations of a test asphalt slab in a wheel tracking test, and the description of the employed wheel loading assumptions for simplifying the FE simulations. Furthermore, a summary of an analysis procedure for the identification of the material parameters associated with the presented constitutive model is given in this section.

3.1 *Geometry of the FE model*

This study simulates the wheel tracking test as an example to investigate the effect of various commonly adapted loading assumptions on rutting predictions. On basis of this analysis, one can draw conclusions about the

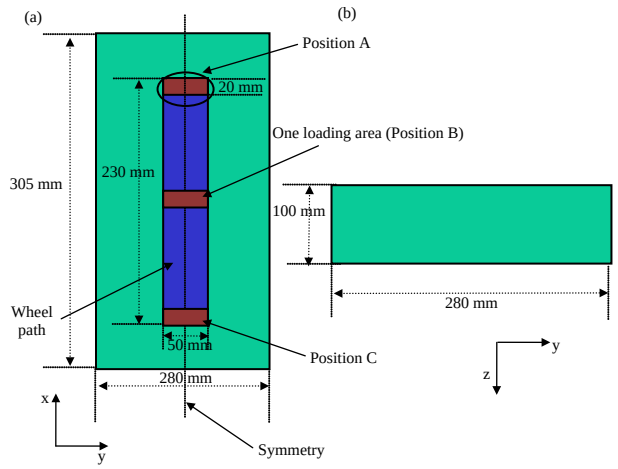

Figure 1. The geometry of the wheel tracking test. The wheel path is shown in blue, whereas the positions at which the rutting value is measured are shown in brown. (a) $X - Y$ plane and (b) $Y - Z$ plane.

suitability and computational cost of each loading assumption in predicting the rutting in asphaltic layers. The geometry of the wheel tracking test is illustrated in Figure 1. The geometry of the wheel tracking test consists of an asphalt slab of dimensions of $305 \times 280 \times 100\,\text{mm}^3$ in length, width and depth, respectively. A wheel load is applied at the middle of the slab along the width and moved back and forth along the length of the slab. The wheel moves with a speed of 40 passes per minute over a wheel path of 230-mm length, which is equivalent to a 0.55 km/h speed. The wheel loading area is assumed as a rectangular shape with dimensions of $20 \times 50\,\text{mm}^2$ in width and length, respectively. The employed asphalt layer, dimensions of the loading area and the wheel speed are from the wheel tracking test conducted by Hunter *et al.* (2007). The loading is applied as a step load within each loading cycle. On account of the symmetric nature of the wheel loading condition and the slab's geometry, the FE model can be reduced to half of the slab by constraining the horizontal direction on the vertical edge of the model to represent the middle of the slab.

The 3D and 2D FE meshes showing the applied wheel loading are shown in Figure 2(a) and (b), respectively. The boundary conditions in both 2D and 3D FE models are imposed such that the horizontal direction on the opposite side of the symmetric boundary is fixed, whereas the bottom of the slab is fixed in the vertical direction. The used element types in the 2D FE simulations in Abaqus are plane strain four-node element with reduced integration (CPE4R) for plane strain analysis and axisymmetric four-node element with reduced integration (CAX4R) for axisymmetric analysis, whereas 3D eight-node element with reduced integration (C3D8R) is used for conducting 3D FE simulations. Moreover, a maximum element aspect ratio of 2 is used for the 2D and 3D elements, respectively. According to the convergence studies for the 2D simulations, $2.5 \times 2.5\,\text{mm}^2$ elements are used under and close to the loads, whereas the maximum element size of $5 \times 5\,\text{mm}^2$ is used for the area far from the loading path. For the 3D simulations, $2.5 \times 2.5 \times 2.5\,\text{mm}^3$ elements are used under the load and close to loading path, whereas the maximum element size of $5 \times 5 \times 5\,\text{mm}^3$ is used for the regions that are far from the loading path. From a convergence study that is not reported here, the constructed 2D and 3D meshes were sufficient to get converged results that are independent of the mesh density. The loading level is 770 kPa and is applied on the top of the asphalt layer with different loading scenarios as described in the next section. For simplicity, the shape of the applied load is assumed to be rectangular. Moreover, frictional and tangential loadings from the contact of the wheel with the asphalt top surface are neglected in this study. These effects and more realistic loading shapes will be considered in a future study.

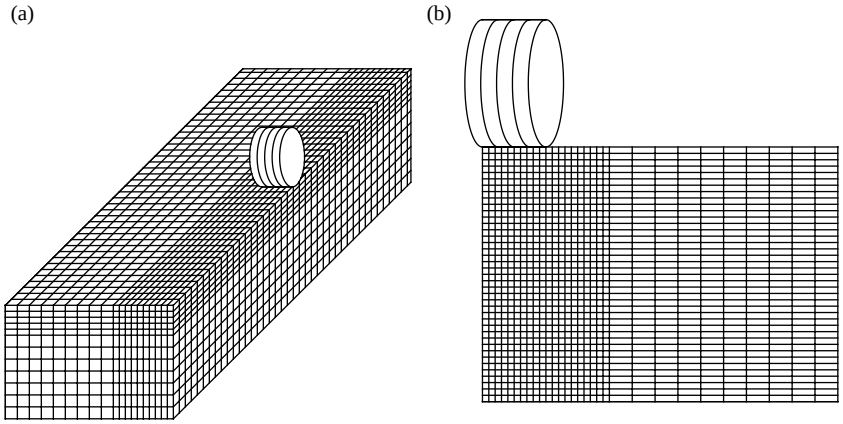

Figure 2. The FE mesh in (a) the 3D simulations and (b) the 2D simulations.

3.2 *Applied wheel loading assumptions*

The loading modes (or loading assumptions) can be categorised into two main types (see Table 1): (1) *loading duration* such as pulse loading, equivalent loading and moving loading and (2) *loading area* such as applying the loading on one wheel area, on the whole wheel path and on a circular loading area that represents the axisymmetric analysis. Considering the combination of those loading categories, four loading modes can be considered in the 2D simulations, whereas seven loading modes can be considered in the 3D simulations (see Table 1). Those loading modes are applied to the 2D and 3D FE models and then the results are compared in terms of the rutting performance in order to find an efficient loading mode, but simple enough, for the prediction of rutting under very large number of repeated loading cycles. Therefore, the objective of simulating these loading scenarios is to identify a loading assumption that allows one to predict effectively and with minimum computational cost the rutting performance of asphaltic layers over a large number of repeated loading cycles without the need for complicated and computationally expensive rutting performance simulations.

3.2.1 *Wheel loading assumptions in the 2D simulations*

In the 2D FE simulations, two cases are considered for the area on which the loading is applied: (1) the loading is applied on an infinite stripe bar along the length of the pavement and (2) the loading is applied on a circular area at the middle of the pavement. The first case is simulated using 2D plane strain FE models, whereas the second case is simulated using 2D axisymmetric FE models. Moreover, two loading durations are assumed for each of the cases. The first loading duration is a pulse loading in which the wheel load is applied with a loading time period of 0.109 s and then the load is removed for 0.109 s as shown in Table 1 and Figure 3. The simulated total loading–unloading cycles in this case are 1000 cycles. The loading scheme is shown in Figure 3(a). The second loading duration is the equivalent loading mode (Mode 2) as shown in Table 1 and Figure 3(b). This loading assumption represents the equivalent loading time by accumulating the loading time from all loading cycles and then applying the wheel loading at once in one loading cycle for the period of accumulated time such that the unloading or resting time is neglected. The advantage of this loading model is that only one step loading is applied instead of applying large number of loading steps, and thus reducing greatly the computational cost. Hence, four loading assumptions are considered in the 2D simulations (see Table 1).

3.2.2 *Wheel loading assumptions in the 3D simulations*

In the 3D FE simulations as compared with the 2D simulations, one can specify the loading location and apply more realistic loading conditions. In the 3D simulations, seven wheel loading scenarios can be simulated. The fifth loading assumption (Mode 5) as shown in Table 1 assumes a pulse loading (as described in Modes 1 and 3) in which the load is applied at the centre of the asphalt layer (position B in Figure 1) with one wheel loading area. As shown in Figure 3, the loading duration is 0.109 s and also 0.109 s for the unloading within each cycle. A 1000 loading–unloading cycles are applied in this case. The sixth loading scenario (Mode 6) assumes an equivalent loading time (as described in Modes 2 and 4) in which one wheel loading area is applied at position B in Figure 1. Loading Modes 7 and 8 assume a pulse loading (loading time of 0.109 s and unloading time of 0.109 s) and an equivalent time loading, respectively. Both Modes 7 and 8 assume the loading over the whole wheel path (shown in Figure 1). Moreover, a circular loading area is assumed for Modes 9 and 10. A pulse loading and an equivalent time loading are assumed for loading Modes 9 and 10, respectively. Finally, the last loading mode is the moving loading (Mode 11) in which the wheel movement is simulated by applying the wheel loading on one set of elements (one loading area) at the beginning of the wheel path (position A in Figure 1). This load remains on the shaded area as shown in Figure 4(a) for 0.109 s ($t_2 - t_1$), and then moves forward to the next set of elements as shown in Figure 4(b). The load remains on the same set of elements as shown in Figure 4(b) for the same loading duration of 0.109 s ($t_3 - t_2$), and then moves to another set of elements as shown in Figure 4(c) until it reaches to the end of the wheel path (position C in Figure 1). This loading mode, which is illustrated in Figure 4, is the most realistic one as compared with the aforementioned loading modes. This approach of simulating the moving load is followed in the current study due to its simplicity and the significant reduction in the computational cost as compared with explicitly simulating a real tyre with considering dynamic effects.

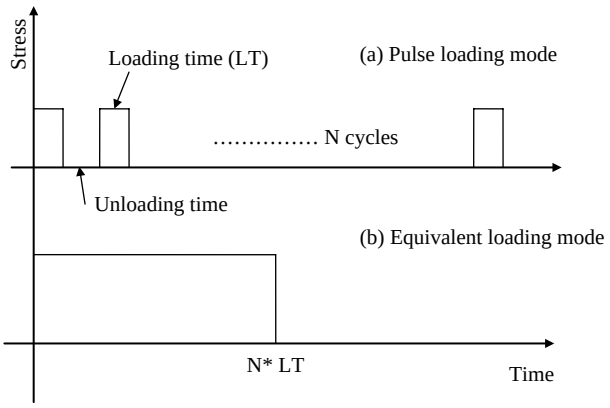

Figure 3. The sketch of equivalent and pulse loading modes. Equivalent loading is obtained by substituting pulse loading by a one step equivalent loading whose duration is equal to the summation of loading times in pulse loading.

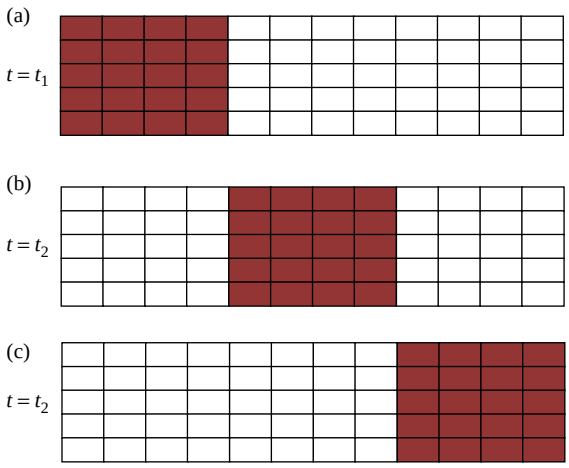

Figure 4. A schematic of the simplified wheel moving loading scenario. The shaded area is the region at which the wheel load is applied over a set of elements and then moved in the traffic direction to a new set of elements.

It should be noted that one would expect different rutting results using plane strain simulations (loading Modes 1 and 2) or using their 3D counterparts (loading Modes 7 and 8) compared with the realistic loading conditions. However, the qualitative comparison of the changes in the results using these simplifications is of great importance in deciding on when to use these simplifications depending on the problem under study.

3.3 *Employed material parameters*

Darabi *et al.* (2011a) used a set of experimental data from University of Nottingham database and identified the model parameters from the creep-recovery and creep tests for the asphalt mixture used in this study. The same model parameters are used in this study. The simulated asphalt mixture is described as a 10-mm Dense Bitumen Macadam (DBM) which is a continuously graded mixture with asphalt binder content of 5.5%. Granite aggregates and an asphalt binder with a penetration grade of 70/100 are used in preparing the asphalt mixtures. Figure 5 shows a flowchart for identifying the constitutive model parameters in a systematic manner. In summary, in order to obtain the asphalt layer viscoelastic and viscoplastic material parameters, creep-recovery experimental data at various stresses, loading times and temperatures were analysed by Abu Al-Rub *et al.* (2009). The first step of the analysis procedure is to obtain the recoverable component (viscoelastic strain), and then the irrecoverable component (viscoplastic strain) can be decoupled by subtracting the recoverable strain from the total strain. As the viscoplastic strain during the recovery process is constant, which is the value at the end of the loading step, the Prony series coefficients ($\bar{D}_n$ and λ_n^0) and the nonlinear parameters g_0, g_1 and g_2 are determined first by analysing the recovery strain at a reference temperature 20°C. Once the Prony series coefficients are obtained, the viscoelastic strain can be calculated, and the viscoplastic strain is then obtained by subtracting the viscoelastic strain from the total strain. From the separated viscoplastic strain, one can identify the corresponding viscoplastic material parameters. More details about the identification of the viscoelastic and viscoplastic material parameters are presented in Abu Al-Rub *et al.* (2009). Once the viscoelastic and viscoplastic material parameters are determined, the viscodamage model parameters can be obtained using the creep test with

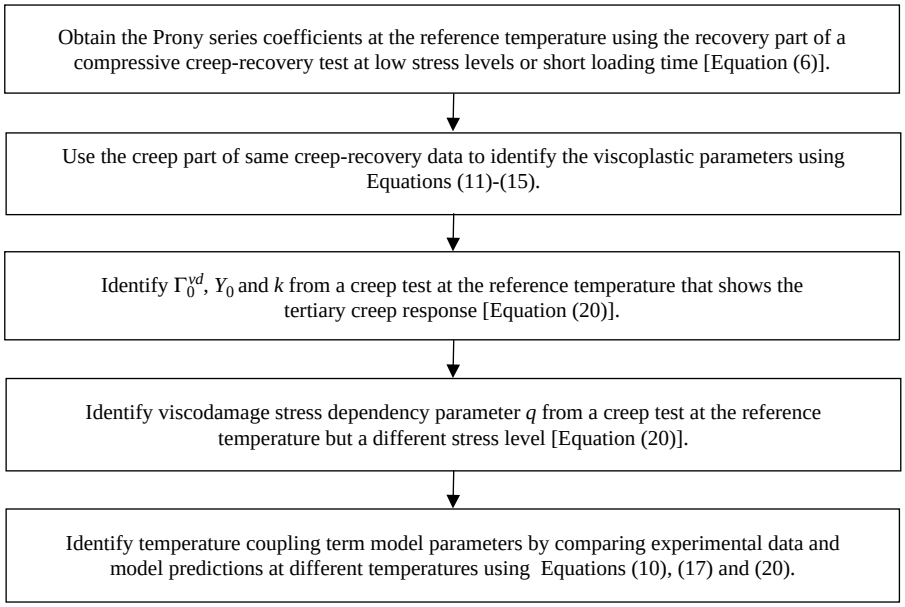

Figure 5. The procedure for identification of the constitutive model parameters.

Table 2. Viscoelastic and viscoplastic material parameters (Abu Al-Rub *et al.* 2009; Darabi *et al.* 2011a).

Viscoelasticity parameters							
N	1	2	3	4	5		
λ_n^0 (s^{-1})	10	1	0.1	0.01	0.001		
$\bar{D}_n$ (kPa^{-1})	1.98×10^{-7}	1.48×10^{-6}	6.56×10^{-7}	1.43×10^{-6}	2.47×10^{-6}		
$\bar{D}_0$ (kPa^{-1})				3.5×10^{-6}			
Viscoplasticity parameters							
α	β	Γ_0^{vp} (s^{-1})	N	κ_0 (kPa)	κ_1 (kPa)	κ_2	d
0.3	0.15	5×10^{-4}	3.63	35	610	215	0.78
Viscodamage parameters							
Γ_0^{vp} (s^{-1})	Y_0 (kPa)	q	k				
4×10^{-5}	700	5	30				

a tertiary creep. Reference damage viscosity (Γ_0^{vd}), reference damage force (Y_0) and model parameter (k) in Equation (20) can be obtained from a creep test at reference temperature and an arbitrary stress level that can be assumed as the reference stress. Once these parameters are determined, the stress-dependency model parameter, q, can be obtained from the experimental data of a creep test at a stress level other than the reference stress and at the reference temperature. More details about the identification of the viscodamage material parameters are presented in Darabi *et al.* (2011a).

Identified viscoelastic, viscoplastic and viscodamage model parameters are listed in Table 2. However, during some preliminary simulations, it is found that the identified viscodamage material parameters in Darabi *et al.* (2011a) did not cause noticeable amount of damage at the largest number of loading cycles simulated in this study. Therefore, in order to investigate the effect of damage evolution on rutting performance predictions, the material parameters for the viscodamage model are modified in such a way that signifies the effect of damage. These assumed material parameters are listed in Table 3.

Moreover, in order to consider the temperature effect on viscoelastic and viscoplastic constitutive equations, the temperature-coupling terms in Equations (10), (17) and (18) are incorporated with a reference temperature of 20°C. The temperature-coupling parameter, δ, can be obtained by comparing the creep tests at different temperatures (Darabi *et al.* 2011a). A value of $\delta = 4.64$ is identified for temperature 40°C, which is used to simulate the rutting performance at 40°C. The listed material parameters in Tables 2 and 3 and the temperature-coupling term parameters are the inputs for simulating the rutting as detailed in the following sections. As the model simulations with damage evolution are conducted only at the reference temperature (20°C), the damage temperature-coupling parameter in Equation (20) is assumed to be 0 ($\xi = 0$).

Table 3. Assumed viscodamage model parameters for inducing early damage growth.

Γ_0^{vp} (s^{-1})	Y_0 (kPa)	q	k
5×10^{-5}	500	1×10^{-5}	300

4. Rutting predictions

Three different constitutive behaviours, elastic–viscoplastic, viscoelastic–viscoplastic and viscoelastic–viscoplastic–viscodamage, are considered here in order to conduct a comprehensive study on the effects of (1) different simplified loading assumptions as listed in Table 1 and (2) different material constitutive behaviours on the 2D and 3D rutting performance predictions of asphaltic layers. The elasto-viscoplastic behaviour is simulated by turning off the viscoelastic and viscodamage constitutive models, whereas the viscoelastic–viscoplastic behaviour is simulated by turning off the viscodamage constitutive model.

As permanent (viscoplastic) displacement is not considered as a degree of freedom at the element's nodes in the classical FE method, it is not possible to calculate permanent surface deformation (i.e. rutting) directly. However, the magnitude of rutting can be calculated numerically by integrating the magnitude of the viscoplastic deformation through the pavement's thickness. This can be achieved by dividing the thickness of the asphalt layer into a number of sub-layers, such that the rutting depth can be calculated as follows:

$$u_{\text{rutting}} = \sum_{i=1}^{k} \varepsilon^{\text{vp}(i)} h^{(i)}, \tag{21}$$

where u_{rutting} is the permanent displacement (rutting), $\varepsilon^{\text{vp}(k)}$ is the vertical viscoplastic strain at ith layer through the depth of the asphalt layer and $h^{(i)}$ is the ith layer thickness. In the following, the rutting is only calculated at the centre of the slab (position B in Figure 1) for the purpose of conducting the numerical comparisons.

4.1 *The 2D FE simulation results*

As it was mentioned in section 3.2.1, four loading scenarios can be assumed for performing the 2D FE

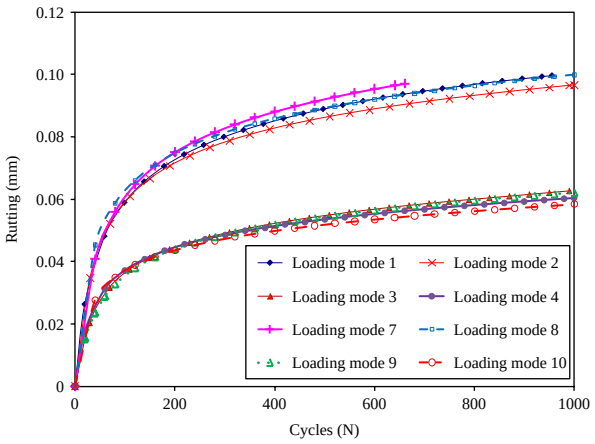

Figure 6. The rutting results for 2D plane strain and axisymmetric and their corresponding 3D FE simulations at temperature 20°C assuming a nonlinear viscoelastic and viscoplastic material constitutive behaviour.

simulations for predicting rutting as shown in Table 1 (i.e. Mode 1, plane strain-pulse loading; Mode 2, plane strain-equivalent loading; Mode 3, axisymmetric-pulse loading and Mode 4, axisymmetric-equivalent loading). In the 2D plane strain simulations, it is assumed that the loading is applied as an infinite strip along the length of the asphalt layer. The corresponding 3D loading modes for the 2D loading Modes 1 and 2 are loading Modes 7 and 8, respectively. Furthermore, for the 2D axisymmetric simulations, the loading is assumed to be applied on a circular area. Hence, the corresponding 3D loading modes for the 2D loading Modes 3 and 4 are loading Modes 9 and 10. Figures 6 and 7 show the rutting vs. loading cycles assuming a viscoelastic–viscoplastic constitutive behaviour at temperatures 20 and 40°C, respectively. Figures 6 and 7 show that the rutting values obtained from the pulse and equivalent loading cases are comparable. However, the difference depends on the employed constitutive model and decreases as the temperature increases. The 2D simulation results assuming an elasto-viscoplastic material behaviour are shown in Figure 8. This figure shows that an elasto-viscoplastic constitutive behaviour leads to prediction of the same rutting values for pulse and equivalent loading cases, when the only difference is the loading duration (i.e. pulse loading vs. equivalent loading). The 2D simulation results for loading Modes 1–4 when damage is activated are shown in Figure 9. Figure 9 shows that when damage is activated, the simulation results for loading Modes 1 and 2 could be very different. This is attributed to the viscous behaviour of the damage law. In other words, changing the loading duration has a significant effect on the value of damage density as the damage law is time dependent. These observations clearly show that the differences in rutting values using different simplified loading assumptions are also model dependent. For example, the time-dependent damage model magnifies the difference between the predicted rutting values when different loading modes are used. Also, one may expect greater differences if other material mechanisms such as the viscoplastic softening (i.e. decreased levels of viscoplastic hardening during each loading cycle due to rearrangements in the material's microstructure) which is related to the loading history are considered. In other words, any material mechanism that is related to the loading history could magnify the differences in calculated rutting values using the simplified loading assumptions and realistic loading scenarios as the simplified loading assumptions do not capture the real loading history. Therefore, it should be emphasised that the rutting predictions from a specific simplified loading assumption

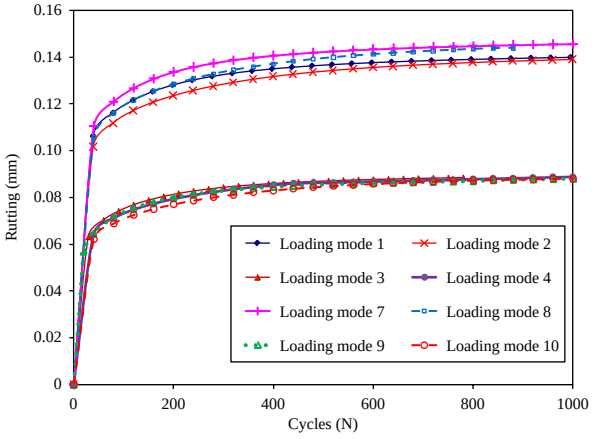

Figure 7. The rutting results for 2D plane strain and axisymmetric and their corresponding 3D FE simulations at temperature 40°C assuming a nonlinear viscoelastic and viscoplastic material constitutive behaviour.

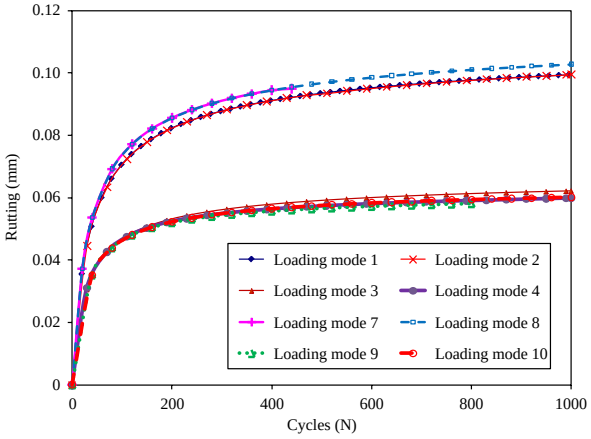

Figure 8. The rutting results for 2D plane strain and axisymmetric and their corresponding 3D FE simulations at temperature 20°C assuming an elasto-viscoplastic material constitutive behaviour.

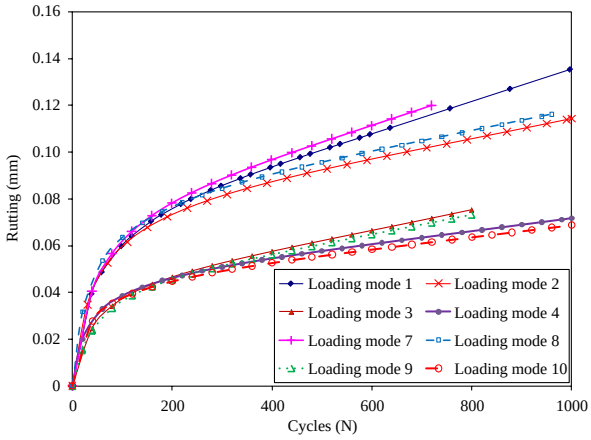

Figure 9. The rutting results for 2D plane strain and axisymmetric and their corresponding 3D FE simulations at temperature 20°C using the coupled viscoelastic–viscoplastic–viscodamage material constitutive model.

completely depend on the employed constitutive model and one cannot generalise the conclusions from a specific loading assumption independent of the employed constitutive model.

The same trend is also obtained from the simulation results of loading Modes 3 and 4. The results of loading Modes 7 and 8, which are the 3D counterparts of loading Modes 1 and 2, respectively, are also presented in Figures 6–9. These figures show that the results of loading Modes 1 and 7, and the results of loading Modes 2 and 8 are very similar. Details of the 3D simulations are presented in the following section.

As an example, the viscoplastic strain and damage density distribution contours after 600 loading cycles for loading Mode 1 are plotted in Figure 10 for the viscoelastic–viscoplastic–viscodamage model. Figure 10(a) shows that the maximum viscoplastic strain occurs at the half top portion of the pavement. Figure 10(b) shows that the maximum damage occurs at the top of the middle part of the asphalt layer, which is exactly the region where the maximum viscoplastic strain occurs. However, as it is clear from Figure 10(b), damage does not distribute towards the bottom part of the asphalt layer. Instead, it localises at the top of the middle part of the asphalt layer that eventually causes macro-crack nucleation at that region. These macro-cracks then propagate towards the surface of the asphalt layer.

It is noteworthy that due to the large computational cost, the rutting simulations of this study are conducted up to 1000 loading cycles, which is much lower than the actual number of loading cycles in the wheel tracking tests. Hence, it is not a surprise that the predicted values for the surface rutting are lower than the actual rutting values in the wheel tracking tests that are conducted for huge number of cycles. However, the main purpose of this study is qualitative comparisons of rutting values obtained from different simplified assumptions on the constitutive model and on the imposed loading scenario with the most realistic constitutive model and loading scenario, which are viscoelastic, viscoplastic, viscodamage model and the moving load scenario, respectively, and are used as a reference for qualifying the rutting predictions. Although this study provides a qualitative comparison between different assumptions for low number of loading cycles, the trend for larger number of loading cycles is expected to be similar. The authors are currently working on

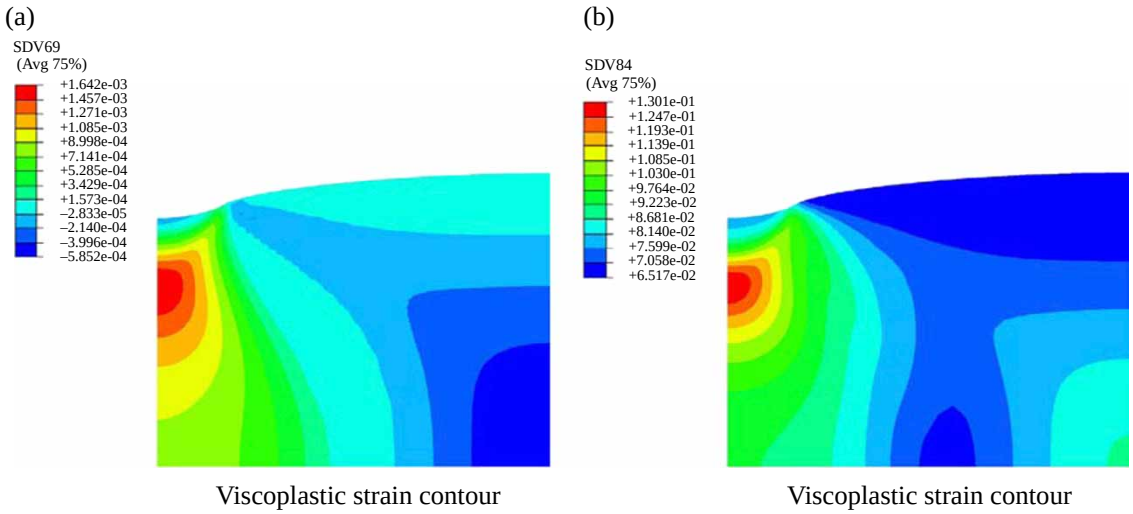

Viscoplastic strain contour Viscoplastic strain contour

Figure 10. Viscoplastic strain and damage density distribution contours after 600 loading cycles for the 2D FE analysis when using the coupled viscoelastic, viscoplastic, viscodamage constitutive model at $T = 20$°C, when the pulse loading scenario is used (loading Mode 1).

developing an extrapolation technique that could be used to extrapolate the 3D simulation results obtained from low number of loading cycles to the simulation results for a large number of loading cycles. This study will be the subject of a future work by the authors.

4.2 *The 3D FE simulation results*

As mentioned in section 3.2.2, seven simplified loading scenarios are simulated for the 3D case. Figures 11 and 12 show the rutting predictions vs. the number of loading cycles at temperatures 20 and 40°C, respectively. These results are obtained assuming that asphalt material behaviour is viscoelastic–viscoplastic with no damage. As the rutting predictions from the moving load (Mode 11) are the closest to the real loading in a wheel tracking test, these figures show that applying the loading over the whole wheel path (Modes 7 and 8) results in a significant error in predicting rutting as compared with the moving load (Mode 11). Figures 11 and 12 show that the axisymmetric assumption also overestimates the rutting value as compared with the most realistic loading mode (Mode 11). However, these figures show that cases for which the wheel loading is only applied on one wheel loading area (Modes 5 and 6) can reasonably predict the simulation results of loading Mode 11. Due to the very large computational cost in conducting the moving load simulations, the results are obtained up to about 400 and 500 cycles at temperatures 20 and 40°C, respectively. In terms of the effect of the pulse and equivalent loading conditions (Mode 5 vs. 6; Mode 7 vs. 8; Mode 9 vs. 10), one can notice from Figures 11 and 12 that the rutting predictions are close when applying Mode 5 vs. Mode 6, Mode 7 vs. Mode 8 and Mode 9 vs. Mode 10.

Figure 13 shows the relationship between the rutting predictions and the number of loading cycles when assuming an elasto-viscoplastic material constitutive behaviour with no viscoelasticity and no damage. Figure 13 shows that using pulse and equivalent loading modes gives comparable predictions when assuming that the loading area is the same. This observation is compatible with the 2D simulation results shown in Figure 8. As inferred from the results in Figures 11 and 12, the rutting predictions from the loading Modes 5 and 6 are close to those from the moving loading mode (Mode 11). However, when assuming loading Modes 7–10 the rutting is over predicted significantly.

In order to study the effect of damage on rutting using different loading modes in the 3D simulations, the viscoelastic–viscoplastic–viscodamage constitutive model is now used. Figure 14 shows the corresponding results at temperature 20°C. It is clear from Figure 14 that the rutting predictions are different for each loading mode and the difference increases as damage grows. Also,

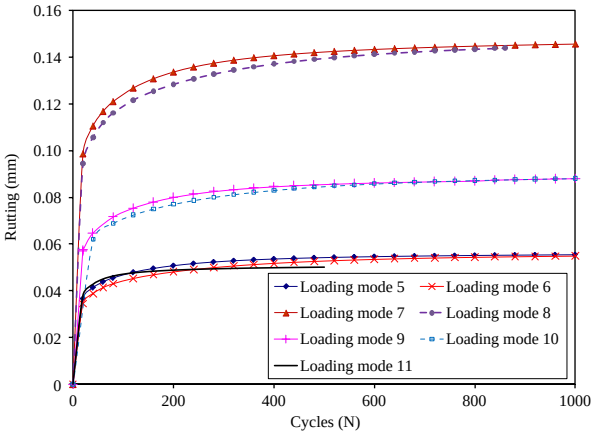

Figure 12. The rutting simulation results from 3D FE analysis at temperature 40°C assuming a nonlinear viscoelastic and viscoplastic material constitutive behaviour.

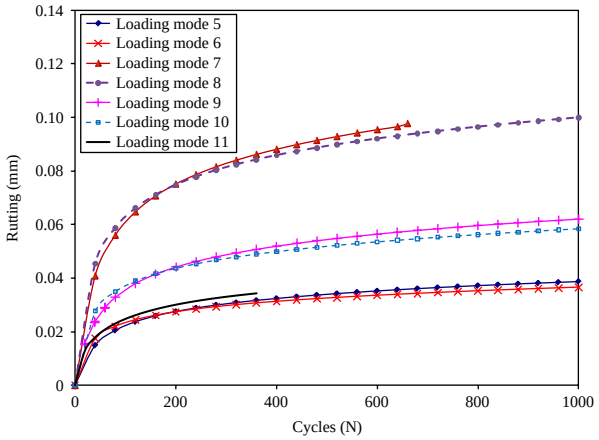

Figure 11. The rutting simulation results from 3D FE analysis at temperature 20°C assuming a nonlinear viscoelastic and viscoplastic material constitutive behaviour.

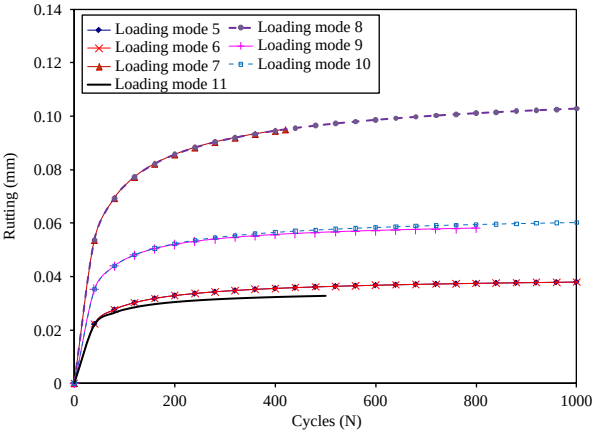

Figure 13. The rutting simulation results from 3D FE analysis at temperature 20°C assuming an elasto-viscoplastic material constitutive behaviour.

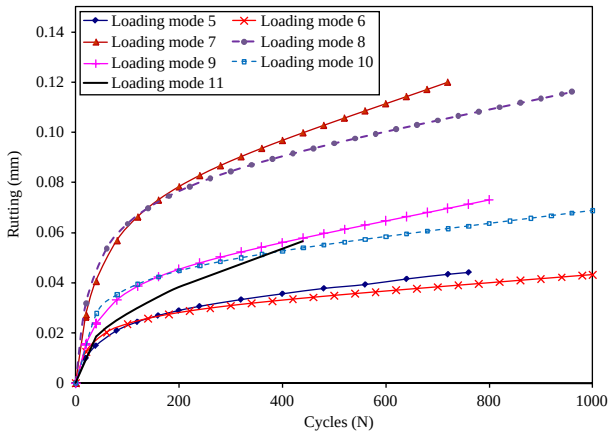

Figure 14. The rutting simulation from 3D FE analysis at temperature 20°C using the coupled viscoelastic–viscoplastic–viscodamage material constitutive model.

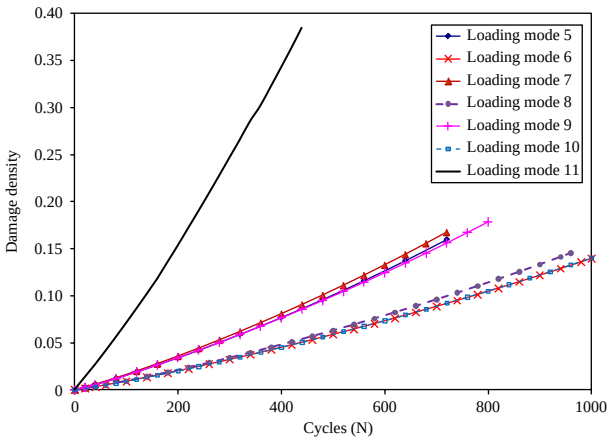

Figure 15. The evolution of the damage density from 3D FE analysis at temperature 20°C using the coupled viscoelastic–viscoplastic–viscodamage material constitutive model.

Figure 14 shows that when damage is activated, results from loading Mode 11 (i.e. moving load) significantly deviate from the results of loading Modes 5 and 6 as compared with those in Figures 11–13. This is attributed to the viscous behaviour of the damage law. In other words, changing the loading duration has a significant effect on the value of damage density as the damage law is time dependent. Moreover, as mentioned in section 3.3, during some preliminary simulations, it is found that the identified viscodamage material parameters in Darabi *et al.* (2011a) did not cause noticeable amount of damage at the largest number of loading cycles simulated in this study. Therefore, in order to investigate the effect of damage evolution on rutting performance predictions, the material parameters for the viscodamage model are modified in such a way that signifies the effect of damage. These assumed material parameters also contribute in magnifying the differences in the predicted rutting values using loading Modes 5 and 6. The total loading duration for loading Mode 11 is larger than the loading duration for other loading modes and, therefore, the rate of rutting accumulation and damage density from loading Mode 11 are greater than those from other loading modes (i.e. Modes 5–10). Figure 15 shows the evolution of the maximum damage density (occurring at the centre of the loading and 30 mm from the top surface) for different loading modes, where the damage density evolves differently depending on the loading model and loading duration, but is much more important for loading Mode 11 that causes the noticeable deviation from loading Modes 5–10. Hence, one can conclude that it is not accurate to substitute the pulse loading with equivalent loading in the presence of significant damage. Also, substitution of loading Mode 11 (moving load) with loading Modes 5 and 6 may cause significant error when damage is activated. Figure 16 compares the rutting predictions for loading Mode 11 when different constitutive models are used. These results show that the effect of using different loading assumptions totally depends on the material constitutive model adapted for conducting the rutting simulations.

As an example, the contour of the viscoplastic strain and damage density distribution after 600 loading cycles for the loading Mode 7 is plotted in Figure 17. Figure 17(a) shows that the maximum viscoplastic strain occurs at the top of the middle part of the asphalt layer, which is consistent with the 2D predictions in Figure 10(a) and previous studies (see e.g. Kim *et al.* 2006). Moreover, it also shows that as the number of loading cycles increases, the compressive viscoplastic strain extends towards both top and bottom of the pavement, which contributes to more permanent deformation. Also, damage distribution contours are plotted for the same problem in Figure 17(b), which shows that the maximum damage occurs at the top

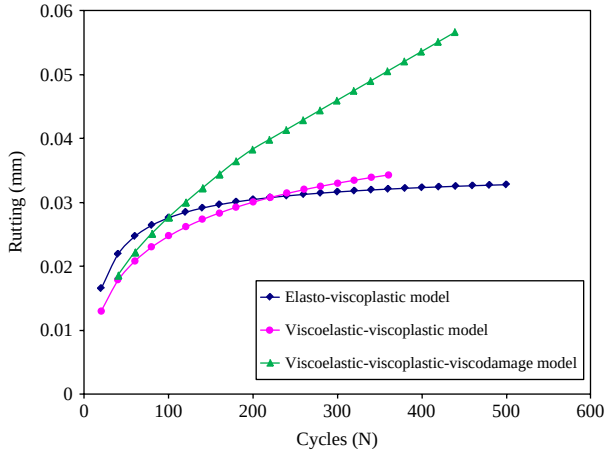

Figure 16. Comparing the rutting predictions from the 3D FE simulations using different constitutive models at temperature 20°C for loading Mode 11.

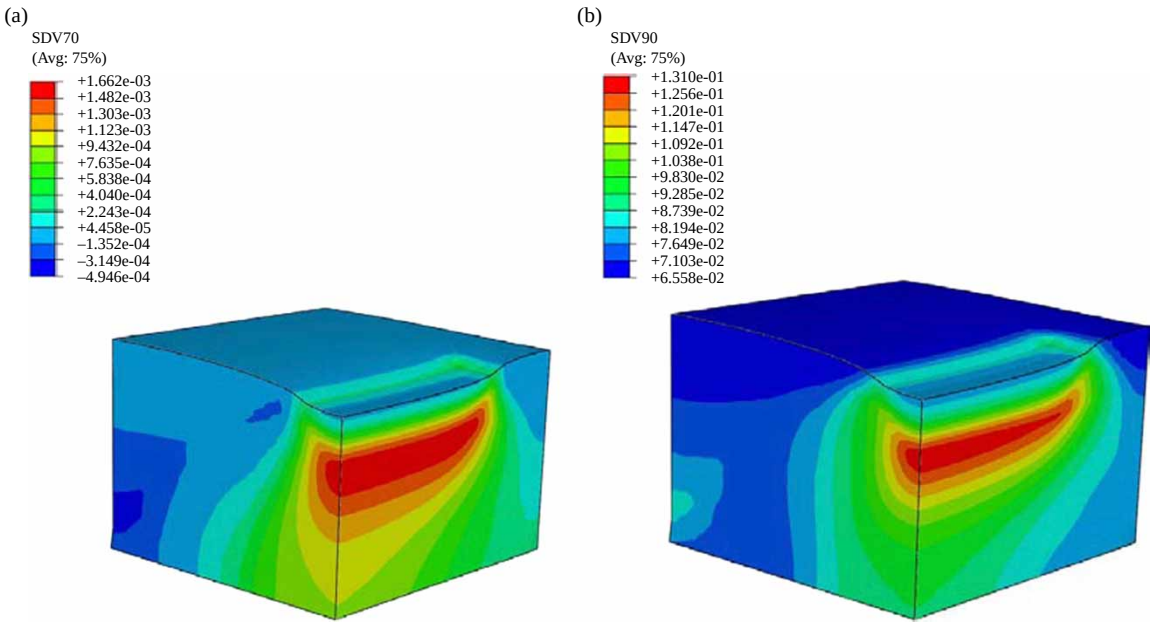

Figure 17. Viscoplastic strain and damage density distribution contours after 600 loading cycles for the 3D FE analysis when using the coupled viscoelastic, viscoplastic, viscodamage constitutive model at $T = 20^{\circ}\mathrm{C}$ when the pulse loading scenario is used (loading Mode 7).

of the middle part of asphalt layer, which is exactly the region where the maximum viscoplastic strain occurs. The results in Figure 17 are consistent with the 2D viscoplasticity and damage contours (Figure 10).

From the 3D FE predictions of rutting (Figures 11–14), one can conclude that the simplified loading and constitutive assumptions can significantly affect the rutting predictions. The difference between the rutting values using the moving load (Mode 11), which is the most realistic one, and the rutting values using the equivalent loading mode (Mode 8), which is the most common loading assumption in the literature, exceeds 100% in some cases. Moreover, assuming equivalency between the pulse loading modes (Modes 7 and 9) and the equivalent loading modes (Modes 8 and 10) totally depends on the assumed constitutive model. This assumption yields almost similar results for an elasto-viscoplastic constitutive model. It could also be reasonable for a viscoelastic–viscoplastic constitutive mode; however, special care should be taken in the presence of damage as the results of these two loading cases could be totally different, depending on the damage level.

The conducted simulations show that rutting predictions in asphaltic pavements using the simplified assumptions such as the 2D analysis instead of the 3D analysis and using the equivalent loading assumption instead of the pulse loading assumption will significantly overestimate rutting, but, on the other hand, significantly reduce the computational cost. However, due to the very large computational cost needed to predict the rutting using 3D FE simulations with a complex coupled viscoelastic, viscoplastic and viscodamage constitutive mode, it is imperative that an extrapolation technique to very large number of cycles is developed based on 3D FE simulations. This will be the focus of a future research by the authors.

5. Summary and conclusions

In this paper, the FE prediction of rutting, which is one of the most challenging and important distresses in asphalt pavements, is investigated thoroughly. The effect of different loading and constitutive behaviour assumptions that greatly simplify the rutting performance predictions in asphalt pavements is systematically investigated. Three material constitutive behaviours are considered for studying the effects of viscoelasticity, viscoplasticity and viscodamage models on the rutting depth in the wheel tracking test. The 2D and 3D FE simulations with different loading assumptions are simulated to study the difference between 2D and 3D simulations and to study the effect of different performance loading assumptions (e.g. pulse loading and equivalent loading) on the predicted rutting depth.

Simulation results show that certain simplified loading scenarios significantly overestimate the rutting performance. It is shown that the 2D simulations significantly

overestimate the rutting depth as compared with the 3D moving loading case, which is the most realistic case considered in this study. It is also shown that the accuracy of the assumption of equivalency between the pulse loading and the equivalent time loading, which has been extensively assumed by many researchers in predicting rutting, totally depends on the assumed material constitutive behaviour (i.e. elasto-viscoplastic, viscoelastic–viscoplastic or viscoelastic–viscoplastic–viscodamage). Therefore, one cannot generalise the conclusions from a specific loading assumption independent of the employed constitutive model. The pulse loading and equivalent time loading simplifications give comparable rutting predictions when the wheel loading is applied on the same area of the wheel's path and when the damage evolution is neglected. Therefore, depending on the level of damage, the results can deviate progressively as damage grows.

The effects of more realistic wheel–pavement contact stresses and the wheel speed will be investigated in the near future by the present authors. Moreover, an extrapolation technique for estimating the rutting depth at large number of loading cycles will be developed based on more realistic 3D rutting performance simulations.

Acknowledgements

The authors acknowledge the financial support provided by the Federal Highway Administration through the Asphalt Research Consortium, and the partial financial support by the Qatar National Research Fund. Also, the authors acknowledge the helpful comments by the anonymous reviewers who helped in making the paper more complete.

References

Abaqus, 2008. *Abaqus Version 6.8*. Providence, RI: Habbit, Karlsson and Sorensen, Inc.

Abu Al-Rub, R.K. and Voyiadjis, G.Z., 2003. On the coupling of anisotropic damage and plasticity models for ductile materials. *International Journal of Solids and Structures*, 40, 2611–2643.

Abu Al-Rub, R.K., Masad, E.A., and Huang, C.W., 2009. *Improving the sustainability of asphalt pavements through developing a predictive model with fundamental material properties*, Final Report submitted to Southwest University Transportation Center, Report # SWUTC/08/476660-0007-1.

Abu Al-Rub, R.K., *et al.*, 2010a. A micro-damage healing model that improves prediction of fatigue life in asphalt mixtures. *International Journal of Engineering Science*, 48, 966–990.

Abu Al-Rub, R.K., Masad, E.A., and Graham, M., 2010b. *Physically-based model for predicting the susceptibility of asphalt pavements to moisture-induced damage*, Final Report submitted to Southwest University Transportation Center, Report # SWUTC/09/476660-0012-1.

Chaboche, J.L., 2003. Damage mechanics. *Comprehensive Structural Integrity*, 2, 213–284.

Chehab, G., 2002. *Characterization of asphalt concrete in tension using a viscoelastic model*. Thesis (PhD). North Carolina State University, Raleigh, NC.

Chehab, G., *et al.*, 2002. Time temperature superposition principle for asphalt concrete mixtures with growing damage in tension state. *Asphalt Paving Technology*, 71, 559–593.

Chehab, G.R., *et al.*, 2003. Characterization of asphalt concrete in uniaxial tension using a viscoelastoplastic model. *Asphalt Paving Technology, AAPT*, 72, 315–355.

Chen, R.S., Tu, C.Y., and Tsai, H.S., 1993. The effect of moisture upon the optimal temperature path of the viscoelastic symmetric composite laminates after post cure. *Journal of Composite Materials*, 27, 1578–1597.

Cho, Y., McCullough, B.F., and Weissmann, J., 1996. Considerations on finite-element method application in pavement structural analysis. *Transportation Research Record*, Transportation Research Board, Washington, DC, 1539, 96–101.

Collop, A.C., *et al.*, 2003. Development and finite element implementation of stress-dependent elastoviscoplastic constitutive model with damage for asphalt. *Transportation Research Record*, Transportation Research Board, Washington, DC, 1832, 96–104.

Darabi, M.K., *et al.*, 2011a. A thermo-viscoelastic-viscoplastic-viscodamage constitutive model for asphaltic materials. *International Journal of Solids and Structures*, 48, 191–207.

Darabi, M.K., *et al.*, 2011b. Thermodynamic based model for coupling temperature-dependent viscoelastic, viscoplastic, and viscodamage constitutive behavior of bituminous materials. *International Journal for Numerical and Analytical Methods in Geomechanics*, 10.1002/nag.1030.

Gibson, N.H., 2006. *A viscoelastoplastic continuum damage model for the compressive behavior of asphalt concrete*. Thesis (PhD). University of Maryland, College Park, MD.

Gibson, N.H., *et al.*, 2003. Viscoelastic, viscoplastic, and damage modeling of asphalt concrete in unconfined compression. *Transportation Research Record*, 1860, 3–15.

Haj-Ali, R.M. and Muliana, A.H., 2004. Numerical finite element formulation of the Schapery non-linear viscoelastic material model. *International Journal for Numerical Methods in Engineering*, 59, 25–45.

Hua, J., 2000. *Finite element modeling and analysis of accelerated pavement testing devices and rutting phenomenon*, Dissertation. Purdue University, USA.

Hua, J. and White, T., 2002. Study of nonlinear tire contact pressure effects on HMA rutting. *International Journal of Geomechanics, ASCE*, 2, 353–376.

Huang, H., 1995.*Analysis of accelerated pavement tests and finite element modeling of rutting phenomenon*, Dissertation. Purdue University, USA.

Huang, C.W., 2008. *Development and numerical implementation of nonlinear viscoelastic-viscoplastic model for asphalt materials*, Thesis (PhD). Texas A&M University, College Station, TX.

Huang, B., Mohammad, L.N., and Rasoulian, M., 2001. Three-dimensional numerical simulation of asphalt pavement at Louisiana accelerated loading facility. *Transportation Research Record*, Transportation Research Board, Washington, DC, 1764, 44–58.

Huang, C.W., *et al.*, 2007. Nonlinear viscoelastic analysis of asphalt mixtures subjected to shear loading. *Mechanics of Time Dependent Materials*, 11, 91–110.

Huang, C.W., *et al.*, 2011. Three dimensional simulations of asphalt pavement performance deformation using a nonlinear viscoelastic and viscoplastic model. *ASCE Journal of Materials in Civil Engineering* 23, 56–68.

Hunter, A.E., Airey, G.D., and Harireche, O., 2007. Numerical modeling of asphalt mixture wheel tracking experiments.

International Journal of Pavement Engineering and Asphalt Technology, 8, 52–71.

Kettil, P., *et al.*, 2007. Simulation of inelastic deformation in road structures due to cyclic mechanical and thermal loads. *Computers and Structures*, 85, 59–70.

Kim, Y.R. and Chehab, G.R., 2002. Advanced characterization of asphalt concrete in uniaxial tension using a viscoelastoplastic model. *Superpave Support and Performance Models Management*, NCHRP 9-19, Task F Report, North Carolina State University, Raleigh, NC.

Kim, Y.R., *et al.*, 2006. Perpetual pavement evaluation using the viscoelastic continuum damage finite element program. *Proceedings of the 2006 International Conference on Perpetual Pavement*. Columbus, OH.

Kim, Y., Allen, D.H., and Little, D.N., 2007. Computational constitutive model for predicting nonlinear viscoelastic damage and fracture failure of asphalt concrete mixtures. *International Journal of Geomechanics*, 7, 102–110.

Lee, H.J. and Kim, Y.R., 1998. A uniaxial viscoelastic constitutive model for asphalt concrete under cyclic loading. *Journal of Engineering Mechanics*, 124, 32–40.

Lemaitre, J. and Chaboche, J.-L., 1990. *Mechanics of solid materials*. London: Cambridge University Press.

Lu, Y. and Wright, P.J., 1998. Numerical approach of visco-elastoplastic analysis for asphalt mixtures. *Computers and Structures*, 69, 139–157.

Masad, E., *et al.*, 2005. Viscoplastic modeling of asphalt mixtures with the effects of anisotropy, damage, and aggregate characteristics. *Journal of Mechanics of Materials*, 37, 1242–1256.

Masad, E., Dessouky, S., and Little, D., 2007. Development of an elastoviscoplastic microstructural-based continuum model to predict permanent deformation in hot mix asphalt. *International Journal of Geomechanics*, 7, 119–130.

Masad, E., *et al.*, 2008. Nonlinear viscoelastic analysis of unaged and aged asphalt binders. *Construction and Building Materials*, 22, 2170–2179.

Masad, E., *et al.*, 2009. Characterization of asphalt binder resistance to permanent deformation based on nonlinear viscoelastic analysis of multiple stress creep recovery (MSCR) test. *Journal of the Association of Asphalt Paving Technologist*, 78, 471–501.

Muliana, A. and Haj-Ali, R., 2004. A multi-scale constitutive formulation for the nonlinear viscoelastic analysis of laminated composite materials and structures. *International Journal of Solids and Structures*, 41, 3461–3490.

Pappas, G. and Rao, V.N.M., 1989. Effects of temperature and moisture content on the viscoelastic behavior of cowpeas. *Journal of Texture Studies*, 20, 393–407.

Park, D.W., Epps Martin, A., and Masad, E.A., 2005. Effects of nonuniform tire contact stresses on pavement response. *Journal of Transportation Engineering, ASCE*, 873–879.

Perl, M., Uzan, J., and Sides, A., 1983. Visco-elasto-plastic constitutive law for bituminous mixture under repeated loading. *Transportation Research Record*, Transportation Research Board, Washington, DC, 911, 20–26.

Perzyna, P., 1971. Thermodynamic theory of viscoplasticity. *Advances in Applied Mechanics*, 11, 313–354.

Saadeh, S. and Masad, E., 2010. On the relationship of microstructure properties of asphalt mixtures to their constitutive behavior. *International Journal of Materials and Structural Integrity*, 4, 186–214.

Sadd, M.H., Parameswaran, D.Q., and Shukla, A., 2004. Simulation of asphalt materials using finite element micromechanical model with damage mechanics. *Transportation Research Record*, Transportation Research Board, Washington, DC, 1832, 86–95.

Saleeb, A., *et al.*, 2005. Numerical simulation techniques for HMA rutting under loaded wheel tester. *The International Journal of Pavement Engineering*, 6 (1), 57–66.

Schapery, R.A., 1969. On the characterization of nonlinear viscoelastic materials. *Polymer Engineering and Science*, 9, 295–310.

Schapery, R.A., 1975. A theory of crack initiation and growth in viscoelastic media, Part I: theoretical development, Part II: approximate methods of analysis, Part III: analysis of continuous growth. *International Journal of Fracture*, 11 141–159, 369–388, 549–562.

Schapery, R.A., 1987. Deformation and fracture characterization of inelastic composite materials using potentials. *Polymer Engineering and Science*, 27, 63–76.

Schapery, R.A., 1999. Nonlinear viscoelastic and viscoplastic constitutive equations with growing damage. *International Journal of Fracture*, 97, 33–66.

Seibi, A.C., *et al.*, 2001. Constitutive relations for asphalt concrete under high rates of loading. *Transportation Research Record*, Transportation Research Board, Washington, DC, 1767, 111–119.

Sides, A., Uzan, J., and Perl, M., 1985. A comprehensive visco-elastoplastic characterization of sand-asphalt under compression and tension cyclic loading. *Journal of Testing and Evaluation*, 13, 49–59.

Sullivan, R.W., 2008. Development of a viscoelastic continuum damage model for cyclic loading. *Mechanics of Time-Dependent Materials*, 12, 329–342.

Underwood, B.S., Kim, Y.R., and Guddati, M.N., 2006. Characterization and performance prediction of ALF mixtures using a viscoelastoplastic continuum damage model. *Asphalt Paving Technology*, 75, 577–636.